Actuation efficiency of nanosecond repetitively pulsed discharges for plasma-assisted swirl flames at pressures up to 3 bar

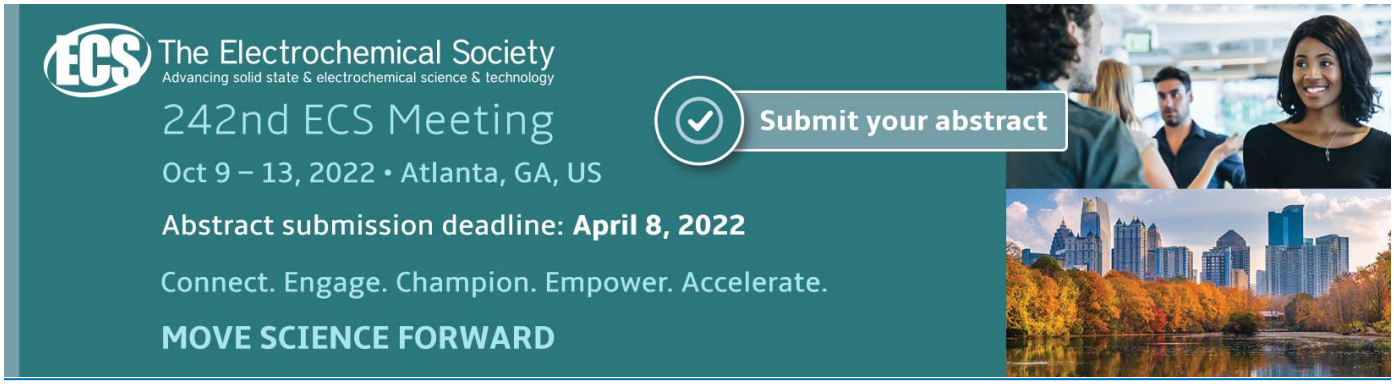

OPEN ACCESS
IOP Publishing
Journal of Physics D: Applied Physics
J. Phys. D: Appl. Phys. **54** (2021) 075208 (11pp)
https://doi.org/10.1088/1361-6463/abc583

Actuation efficiency of nanosecond repetitively pulsed discharges for plasma-assisted swirl flames at pressures up to 3 bar

Francesco Di Sabatino[1], Thibault F Guiberti[1], Jonas P Moeck[2], William L Roberts[1] and Deanna A Lacoste[1]

[1] Clean Combustion Research Center, King Abdullah University of Science and Technology, Thuwal 23955-6900, Saudi Arabia
[2] Norwegian University of Science and Technology, 7491 Trondheim, Norway

E-mail: deanna.lacoste@kaust.edu.sa

Received 26 August 2020, revised 12 October 2020
Accepted for publication 28 October 2020
Published 2 December 2020

Abstract

This study analyzes different strategies of plasma actuation of premixed swirl flames at pressures up to 3 bar. A wide range of applied voltages and pulse repetition frequencies (PRF) is considered, resulting in different combinations of nanosecond repetitively pulsed (NRP) discharge regimes, NRP glow and NRP spark discharges. Electrical characterization of the discharges is performed, measuring voltage and current, and deposited energy and power are evaluated. The effectiveness of the plasma actuation is assessed through images of OH^* chemiluminescence from the flame. From these images, the distance of the center of gravity of the flame to the burner plate is evaluated, with and without plasma actuation. The results show that strategies which involve a high percentage of NRP sparks are effective at improving flame anchoring at atmospheric pressure, while they are detrimental at higher pressures. Therefore, high applied voltage and low PRF are preferable at atmospheric pressure, while the opposite is observed at elevated pressures. Moreover, it is found that a ratio of plasma power to thermal power of the flame around 1% is the best compromise between a strong actuation of the flame and a reasonable deposited electrical power. Explanations for these results are proposed.

Keywords: flame stabilization, non-equilibrium plasma discharges, plasma-assisted combustion, high-pressure combustion.

(Some figures may appear in colour only in the online journal)

1. Introduction

Improving combustion efficiency and reducing pollutant emissions in combustion systems such as gas turbine engines are major challenges that the scientific community is currently facing. In this context, burning fuels in lean premixed condition and at elevated pressure is a strategy widely utilized. However, these burning conditions have limitations, such as unstable combustion and flame blow-off [1]. Finding ways to avoid or mitigate these phenomena in gas turbine combustors

or in high-pressure burners would be of interest for the design of clean combustion systems.

Non-thermal plasmas generated by nanosecond repetitively pulsed (NRP) discharges have been utilized to improve the stability of various types of flames, including lean premixed swirl flames that are widely used in gas turbine combustors [2–12]. However, the vast majority of these studies was carried out at atmospheric pressure, with only two recent papers presenting the effect of NRP discharges on flames at elevated pressures. In [11], Kim and Cohen showed that the lean blow-off limit of methane-air jet flames could be extended by NRP plasma discharges at pressures up to 5 bar. Unfortunately, they found that, with their plasma actuation strategy, the effectiveness of plasma actuation on the flame was decreasing with increasing pressure. As they did not provide any characterization of the discharges, no conclusion on the efficiency of the plasma actuation strategy could be drawn.

In [12], Di Sabatino and Lacoste demonstrated that NRP discharges were efficient in extending the blow-off limit of lean premixed swirl flames at pressures up to 5 bar. They found that the effectiveness of plasma actuation remained almost constant with increasing pressure. Moreover, the plasma discharges were electrically characterized, highlighting that actuation with NRP discharges in the glow regime, known to promote the chemical impact of the plasma, became more efficient than actuation with NRP discharges in the spark regime, with strong thermal and chemical impact, for pressures above 2 bar. This result was not explained. Even though these two studies [11, 12] showed promising results for plasma actuation at elevated pressures, they did not provide extensive parametric analysis, that could, for example, explain the discrepancy in their conclusions concerning the effectiveness of plasma actuation by NRP discharges at elevated pressure. This is the purpose of the present study.

The two main objectives of this study are (1) to compare different plasma actuation settings on the anchoring of lean premixed swirl flames at pressures up to 3 bar, and (2) to suggest effective plasma actuation strategies using NRP discharges for flames at elevated pressure.

2. Experimental setup and methodology

In this section, the experimental setup and diagnostics utilized are briefly presented. Then, the experimental conditions investigated are summarized. Finally, the methodology followed to collect and analyze the data is detailed.

2.1. PACCI burner and HPCD

The experimental setup comprises a swirl burner equipped with a system to generate plasma discharges, referred to as the plasma-assisted control of combustion instabilities (PACCI) burner. A detailed description of the PACCI burner is presented in [13]. The burner is installed in a high-pressure combustion duct (HPCD). A detailed description of the HPCD can be found in [14, 15].

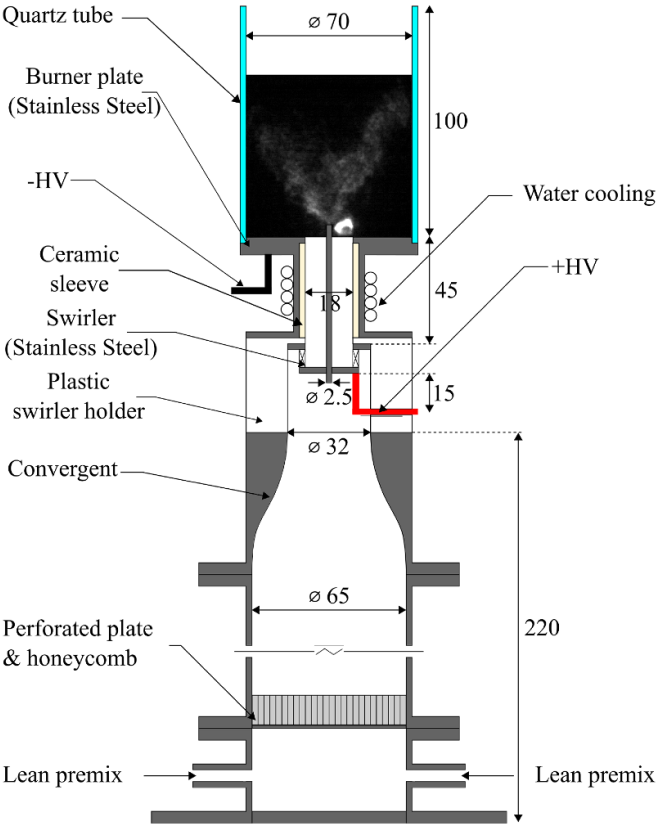

Figure 1. Schematic of the PACCI burner with insert of a single shot OH^* chemiluminescence image of the flame during actuation by NRP sparks at 1 bar. All dimensions in millimeters.

A schematic of the PACCI burner is presented in figure 1. The mixture of methane and air, controlled by mass flow controllers (Brooks SLA58 series), is injected in a plenum, 120-mm long. The accuracy and precision of the mass flow controllers are around 1% of their actual values. Downstream the plenum, the mixture flows through a honeycomb and a perforated plate before entering a radial swirler with a measured swirl number of 0.4. The mixture is injected in the combustion section through an injection tube of 18 mm diameter. A stainless steel rod of 2.5 mm diameter is installed at the center of the injection tube. This rod serves as the anode (positive high-voltage, +HV in figure 1) for the generation of plasma discharges, while the tip of the burner plate surrounding the injection tube serves as the cathode (negative high-voltage, -HV in figure 1). The injection tube is protected by a layer of ceramic material to avoid discharges in unwanted locations. The swirl flame is stabilized in the combustion section, confined by a 100 mm long and 70 mm diameter quartz tube.

The NRP discharges are generated between the stainless steel rod and the inner rim of the burner plate, separated by a gap of 7.75 mm, by applying 20 ns duration high-voltage pulses, at various pulse repetition frequencies (PRF). In-house-designed high-voltage connections are utilized to link the positive and negative outputs of the plasma generator (FID FPD 25-100MC2), located outside of the HPCD, to the

PACCI burner. These connections ensure that the high voltage needed to generate the plasma discharges is safely delivered to the anode and cathode of the burner. Except for the electrodes, all other metallic parts of the PACCI burner are grounded.

The PACCI burner is installed in the HPCD, a large cylindrical vessel of 0.41 m diameter, equipped with multiple ports and optical windows. It can sustain pressures up to 45 bar; however, the maximum pressure used in this study is 3 bar. The pressure is regulated by a back pressure valve, located about 3 m downstream of the PACCI burner. The HPCD is grounded.

2.2. Diagnostics

In this study, the NRP discharges are electrically characterized, and the effect of plasma actuation on the flame is visually assessed.

During plasma actuation of the flame, the applied voltage is measured with voltage probes (Tektronix P6015A) on the positive and negative high-voltage connections, outside of the HPCD. The current is also measured outside of the HPCD, with a current probe (Pearson Current Monitor, Model 6585) on the ground cable. An oscilloscope (Agilent Technologies Infiniium 2.5 GHz) is utilized to simultaneously record the two voltage and the current signals.

Images of the chemiluminescence of excited hydroxyl radicals (OH^*) from the flame are collected with a high-speed CMOS camera (Lavision HSS8) equipped with an intensifier (Lavision IRO), a UV lens (105 mm F/5.6 Coastal Optics), and a 40-nm bandpass filter centered at 310 nm (Lavision 1108 760). These images are utilized to assess the effect of NRP plasma discharges on the average position of the flame.

2.3. Experimental conditions

Three different operating pressures, P_{amb}, are considered in this study: 1, 2, and 3 bar. The average bulk flow velocity, $\bar{V}_{bulk}$, at the exit of the injection tube is maintained constant at 6.8 m s^{-1}, for all the conditions analyzed. The equivalence ratio of the mixture, ϕ, is slightly modified to keep a similar flame shape when the pressure is increased. A photograph of the methane-air swirl flame at 1 bar is presented in figure 2(a).

A summary of the combustion conditions investigated is reported in table 1. The thermal power of the flame is indicated by P_{flame}, and Re is the bulk Reynolds number evaluated at the exit of the injection tube. The distances of the center of gravity of the flame from the burner plate, Z_{COG}, are also reported. They correspond to conditions without plasma actuation. Since $\bar{V}_{bulk}$ is kept constant when the operating pressure is increased, P_{flame} and Re increase with increasing pressure. For example, at 1 bar, $P_{flame} = 4$ kW and Re = 7800, while at 3 bar $P_{flame} = 11.5$ kW and Re = 23,400.

During plasma actuation, the pulse duration is kept constant (about 20 ns). The applied voltage and PRF are the two parameters investigated in this study, for the three pressures considered. The range of applied voltages considered is 8–16 kV, while the range of PRFs is 5–100 kHz.

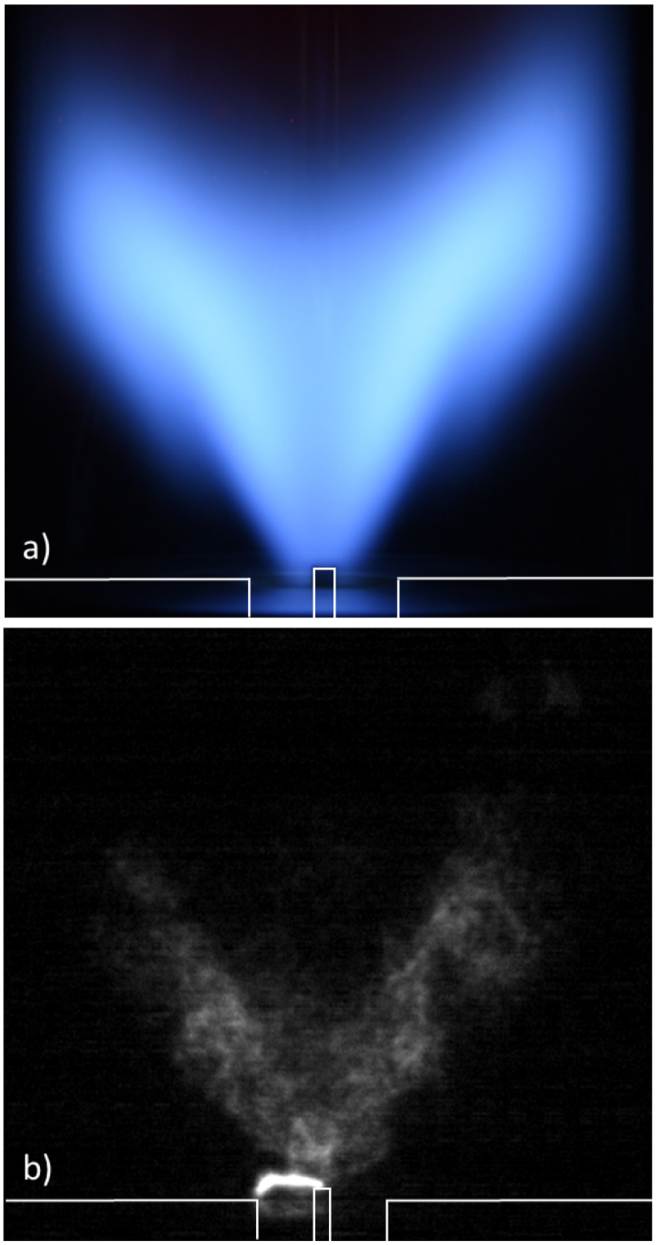

Figure 2. (a) Photograph of the methane–air swirl flame at 1 bar (5 s exposure time). (b) OH^*-chemiluminescence image of the same flame with NRP spark discharges at 10 kHz and 12 kV (90 μs exposure time, synchronized in-between two high-voltage pulses). White lines highlight the burner and rod contours.

2.4. Methodology

The characterization of the plasma discharges and the quantification of their effect on the average flame position are carried out following the procedure detailed here.

After the flame is ignited by a laser-generated spark, the burner is run for 15 min to ensure thermal equilibrium. The plasma actuation is then initiated, for a given applied voltage and PRF. After steady-state is reached (after 10 s of plasma actuation), the temporal evolution of the voltage and current signals is measured for 500 pulses. The applied voltage measured on the cathode is inverted and added to

Table 1. Summary of the experimental conditions.

P_{amb} (bar)	ϕ	P_{flame} (kW)	$\bar{V}_{bulk}$ (m s^{-1})	Re	Z_{COG} (mm)
1	0.67	4.0	6.8	7800	28.1
2	0.65	7.9	6.8	15,600	27.7
3	0.63	11.5	6.8	23,400	27.8

the applied voltage measured on the anode. The resulting waveform is synchronized with the total current waveform. By multiplying the applied voltage and current, the electrical energy deposited by each pulse is determined. The deposited power is evaluated by multiplying the PRF by the average energy deposited over 500 pulses. This procedure is followed for each condition of pressure, applied voltage, and PRF investigated.

The effect of the plasma actuation on the average flame position is quantified by utilizing the images of OH* chemiluminescence. These images are collected after reaching steady state, as defined in the previous paragraph. The camera is synchronized to take images only in-between pulses. However, the OH* filaments generated by the discharges emit for a duration longer than the delay between the pulses (10–200 μs, depending on the PRF). They are so intense compared to the naturally occurring OH* chemiluminescence of the flame that no information could be extracted from the base of the flame, as shown in figure 2(b). The field of view of the camera is then chosen to avoid direct imaging of the plasma filaments that could saturate and damage the camera. Series of 1000 images are collected for each experimental condition, with and without plasma actuation, for each combination of pressure, applied voltage, and PRF. Since different values of PRF are considered, the acquisition frequency and the exposure time of the camera are adjusted accordingly. Moreover, each image is corrected for non-linearities of the camera. Averaging these 1000 images, a mean image of the flame is obtained. It is verified that, even if the total averaging time differs if the PRF is modified, the average flame images of all the experimental conditions are statistically converged. Examples of average flame images, with and without plasma actuation, are reported in figure 3.

The position of the center of gravity (COG) of the flames is estimated from these average images. In the (r, z) plane, such as defined in figure 3, the coordinates of the COG, R_{COG} and Z_{COG}, are obtained from:

$$R_{COG} = \frac{\sum I_i \cdot r_i}{\sum I_i}, \quad Z_{COG} = \frac{\sum I_i \cdot z_i}{\sum I_i}, \tag{1}$$

where I_i is the intensity of the ith pixel of the image, and r_i and z_i are its coordinates. The distance from the COG to the burner plate in the z-direction (Z_{COG}) is utilized as a parameter highlighting the effect of plasma actuation on the average flame position. A detailed analysis of the effect of plasma actuation on the Z_{COG} is presented in the next section.

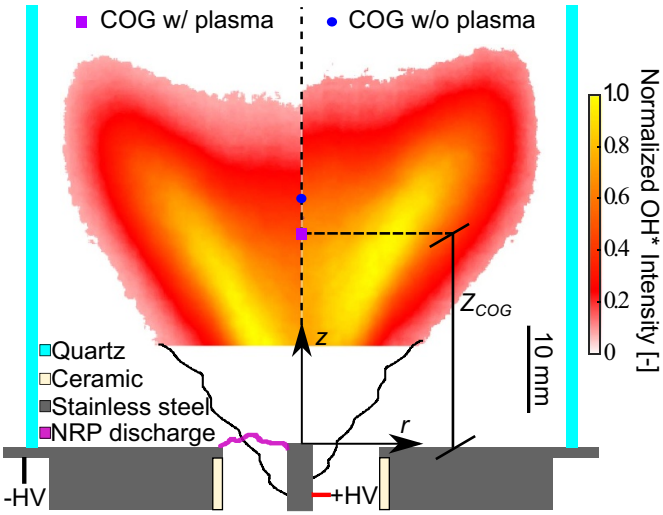

Figure 3. Examples of average OH* chemiluminescence images of a flame with (left) and without (right) plasma actuation, at 1 bar. Plasma actuation is generated by pulses of 12 kV and 10 kHz. The center of gravity (COG) of the two flames as well as Z_{COG} are highlighted. The Z_{COG} without and with plasma actuation are 28 and 24 mm, respectively.

3. Results and discussion

In this section, first the electrical characterization of the NRP discharges is presented. Then, the effect of plasma actuation on the average flame position at different operating pressures is shown and analyzed. Finally, the plasma actuation strategies at different pressures are discussed.

3.1. Electrical properties of the plasma discharges

Depending on the applied voltage and PRF, two discharge regimes can be obtained, namely, NRP glow and the NRP spark discharges, as defined in [16, 17]. The NRP glow discharges mainly have a chemical impact on the flame [18], while NRP spark discharges influence the flame hydrodynamically, thermally, and chemically [19–21]. Examples of the temporal evolution of the voltage, total current, and corresponding deposited energy are presented in figure 4 for NRP glow discharges (a) and NRP spark discharges (b). These waveforms are measured in a flame at 1 bar, for a setting of the plasma generator at 8 kV and a PRF of 50 kHz.

First, it is interesting to note that for a given setting of the plasma actuation, both NRP glow discharges and NRP spark discharges may be observed, with a similar breakdown voltage of about 6 kV (peak voltage in figures 4(a) and (b). This is probably due to the highly complex gaseous media in the inter-electrode area, with a time-varying combination of turbulent fresh mixture, flame front, and burned gases. Depending on the local gas composition at breakdown, the discharges can be either in the glow or spark regime. Note that as the instantaneous energy is calculated utilizing the total current, it is not always increasing with time. Fluctuations of instantaneous energy are induced by the charge and discharge of stray

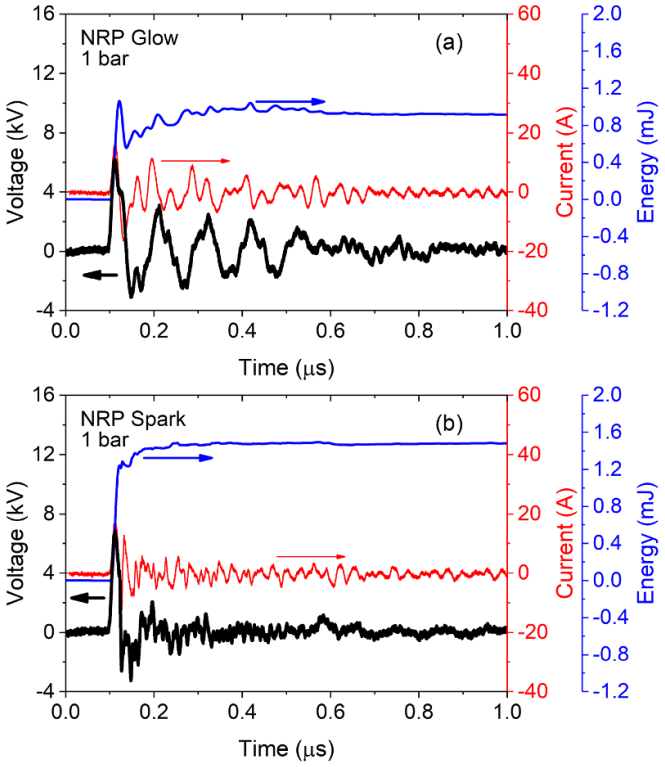

Figure 4. Examples of the temporal evolution of the voltage, current and corresponding energy, obtained for NRP glow discharges (a) and NRP spark discharges (b), generated by pulses of 8 kV applied at 50 kHz, in a flame at 1 bar.

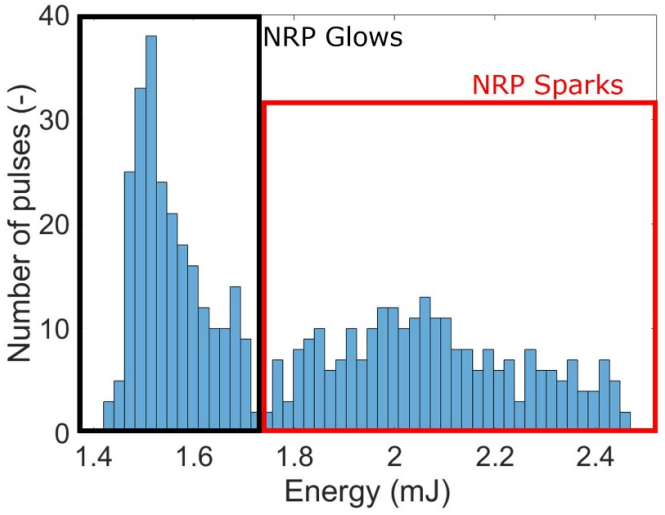

Figure 5. Number of pulses as a function of the energy deposited for 500 NRP discharges produced in a flame at 1 bar for 11 kV applied voltage and a PRF of 10 kHz.

capacitance of the electrical circuit. After about 0.5 μs, the instantaneous energy remains constant, and its value corresponds to the energy deposited by a discharge in the gap. In this example, the NRP spark deposits 1.5 mJ, while the NRP glow only deposits 0.9 mJ. The error induced by using the total current instead of the conductive current has been evaluated by calculating the energy using voltage and current waveforms for conditions for which no discharge was obtained. For all cases, it is below 5% of the energy obtained for the NRP glow discharges. Knowing the PRF and the average deposited energy for the 500 pulses measured, it is possible to determine the average power of the plasma discharges, P_{plasma}, for a given condition. The ratio of P_{plasma} and thermal power released by the flame, P_{flame}, defines the power ratio, P_{ratio}, that is utilized in the analysis of the results in the following sections.

Another quantity of interest extracted from the electrical characterization of the discharges is the percentage of NRP sparks for a given condition. Figure 5 presents an example of distribution of number of pulses as a function of the energy deposited for 500 NRP discharges produced in a flame at 1 bar, for 11 kV applied voltage and 10 kHz PRF. The bi-modal distribution of the pulses allows for a clear distinction between the two discharge regimes.

3.2. *Effect of plasma power and applied voltage on the flame anchoring*

As shown in figure 3, NRP discharges affect the position of the flame. Specifically, the COG of the flame moves towards the burner plate during plasma actuation, and the distance between the COG and the burner, Z_{COG}, is reduced. This anchoring effect is a direct indicator of the plasma actuation because it results from the same plasma effect on the flame as that responsible for reducing the response of a flame to acoustic perturbations [13], or to promote the stabilization of flames close to blow-off [3, 4, 7–10, 12]. Thus, it is interesting to analyze how Z_{COG} evolves during plasma actuation with different combinations of discharge parameters, at different operating pressures.

Figure 6 presents the evolution of Z_{COG} as a function of the power ratio, P_{ratio}, at 1 (a), 2 (b), and 3 bar (c). Since for any plasma actuation, a combination of NRP glows and sparks is obtained, the average deposited energy utilized to calculate P_{ratio} is evaluated considering both discharge regimes. At all pressures, without plasma actuation, $Z_{COG} \approx 28$ mm (see table 1) and when NRP discharges are applied, Z_{COG} decreases. The value of Z_{COG} without plasma actuation is almost constant with increasing the pressure because the equivalence ratio has been adjusted to maintain a similar flame shape for all pressures, as explained in section 2.3. For a given pressure and applied voltage, P_{ratio} is changed by adjusting the PRF, between 5 and 100 kHz (see section 3.5). Note that for the three pressures considered, different ranges of applied voltage are investigated. These ranges result from two limiting conditions: achieving NRP spark discharges and maintaining the integrity of the burner. For example, at 2 bar, for an applied voltage of 9 kV, no NRP spark discharges can be observed, while for an applied voltage of 15 kV, the probability for the flame to flash-back into the injection tube becomes very high. Moreover, the strong NRP sparks produced would quickly damage the electrodes.

For the three pressures studied, at constant applied voltage, Z_{COG} generally decreases with increasing P_{ratio}. However, for a power ratio larger than 1%, this decrease becomes marginal. It is interesting to note that regardless of the pressure,

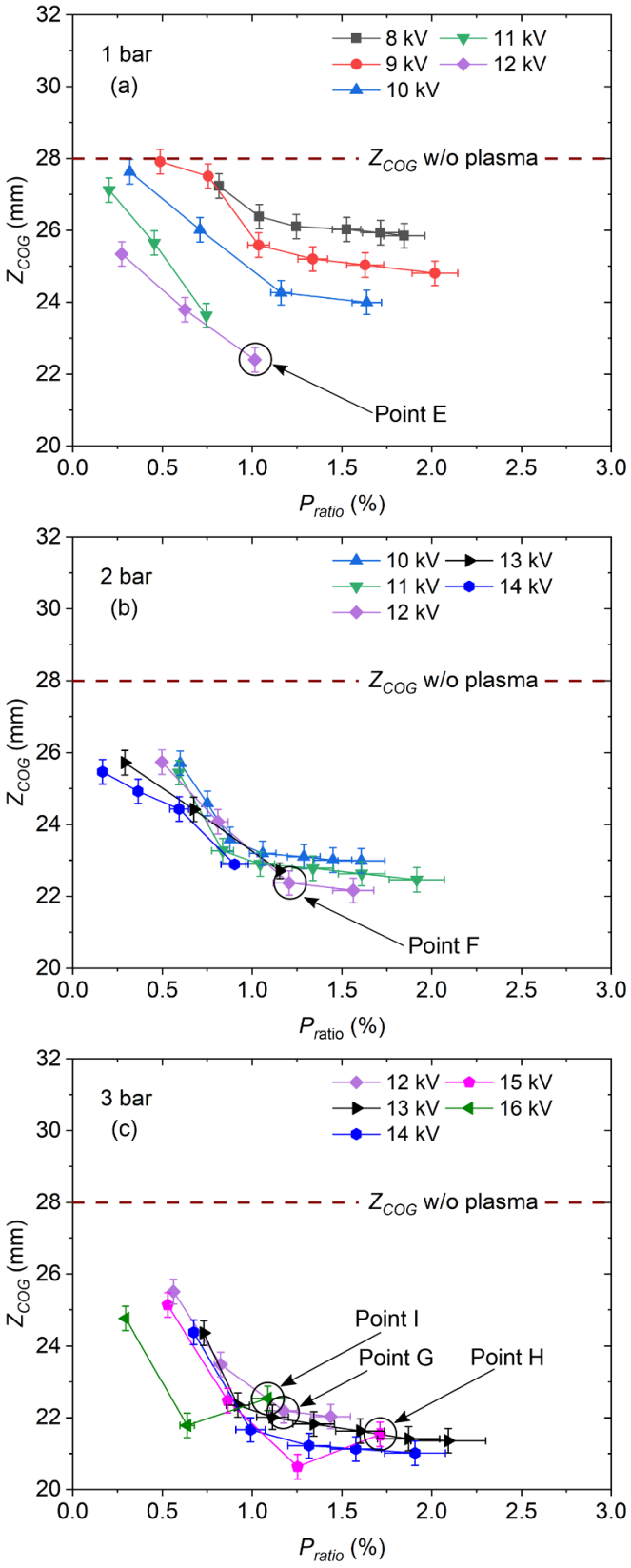

Figure 6. Distance between the burner plate and the center of gravity of the flame, Z_{COG}, as a function of the plasma to flame power ratio, P_{ratio}, at 1 (a), 2 (b), and 3 bar (c) for different applied voltages. The error bars on P_{ratio} represent the standard deviation of the measurements. The error bars on Z_{COG} represent the uncertainty due to the spatial resolution.

Z_{COG} reaches a similar absolute minimum value of 20–22 mm (at 1 bar, Z_{COG} minimum is equal to 22.3 mm, at 2 bar, it is equal to 22.0 mm, and at 3 bar, it is equal to 20.5 mm). This distance corresponds to fully anchored flames. As the shape of the flame is the same at all pressures (thanks to adjustments in the equivalence ratio), Z_{COG} for the fully attached flames takes the same value at all pressures. A smaller value in Z_{COG} would correspond to the beginning of a flash-back of the flame in the injection tube. Moreover, saturation of the plasma effect on the flame might affect the absolute minimum value of Z_{COG}. Additional experiments should be carried out to highlight possible saturation mechanisms in the flame response to plasma forcing. There are two exceptions for the general trend just described: the cases of flame actuation at 3 bar with 15 and 16 kV of applied voltage (pink pentagon and green triangles in figure 6(c), respectively). In these two cases, Z_{COG} first decreases with increasing P_{ratio}, and then increases. An increase in Z_{COG} is an indicator that the flame is less anchored on the burner, *i.e.*, the NRP discharges are less efficient in stabilizing the flame.

Finally, for a given P_{ratio}, at 1 bar, the NRP discharges have an increasing effect on the anchoring of the flame by increasing the applied voltage. For example, for $P_{ratio} = 1\%$, at 8 kV (black squares in figure 6(a), $Z_{COG} = 26.5$ mm, while at 12 kV (violet diamonds in figure 6(a), $Z_{COG} = 22.3$ mm. However, at 2 and 3 bar, for a given P_{ratio}, the effect of applied voltage is less pronounced.

In summary, at all pressures investigated, NRP discharges have an anchoring effect on the swirl flames. Furthermore, increasing the ratio of plasma power to flame thermal power, P_{ratio}, generally increases the effect of the plasma actuation. However, P_{ratio} is not the only parameter controlling the effectiveness of plasma actuation. At atmospheric pressure, for a constant P_{ratio}, an increase in applied voltage increases the effect of the plasma, while at 3 bar, an increase in applied voltage can have a reverse effect on the flame anchoring. The effect of applied voltage on the plasma actuation efficiency is discussed in the next section.

3.3. *Effect of applied voltage on the actuation efficiency*

At a given pressure, an increase in applied voltage increases both the percentage of NRP spark discharges versus NRP glow discharges and the average energy per pulse. Therefore, to obtain a constant P_{ratio}, the PRF has to be decreased and, consequently, the delay between discharges increases. This increase in stronger and sparser discharges could explain the results on the effect of the applied voltage, positive or negative, on the flame anchoring presented in figure 6.

Figure 7 presents the percentage of NRP sparks obtained for 500 discharges as a function of P_{ratio} and applied voltage, for the three pressures considered. For a given P_{ratio}, the range of percentages of NRP spark discharges obtained for the different values of applied voltage is larger at 1 bar than at higher pressures. For example, for $P_{ratio} = 1\%$, the percentage of NRP sparks ranges from 5% at 8 kV to 90% at 12 kV, while at 2 bar,

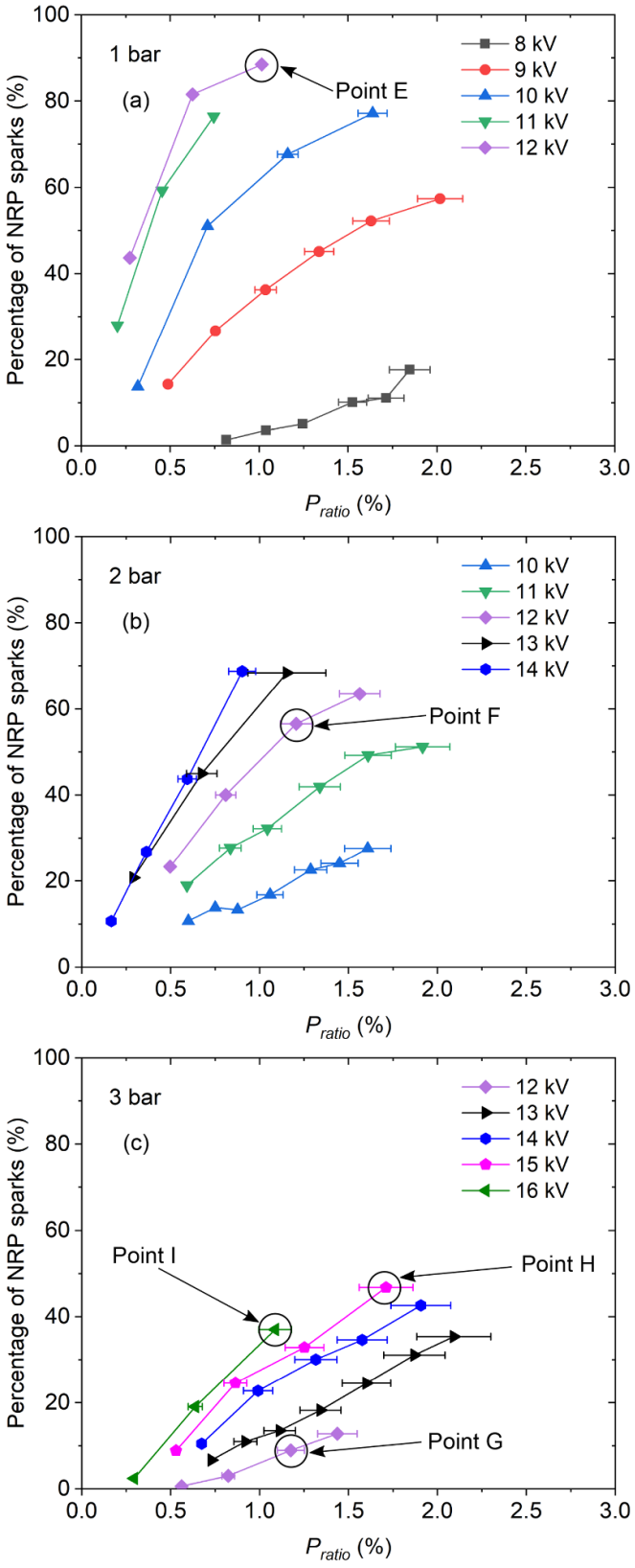

Figure 7. Percentage of NRP sparks for 500 pulses as a function of power ratio at 1 (a), 2 (b), and 3 bar (c) for different applied voltage. The error bars represent the standard deviation of the measurement.

it ranges from from 15% at 10 kV to 70% at 13 kV, and at 3 bar, from 5% at 12 kV to 40% at 16 kV.

At 1 bar, for $P_{\text{ratio}} = 1\%$, the most efficient plasma actuation is obtained for 12 kV (Point E in figures 6(a) and 7(a)). This actuation is obtained for 90% of NRP sparks. For an actuation with mainly NRP glow discharges, for example at 8 kV with 5% of NRP sparks, the plasma effect on the flame anchoring becomes weaker; less than a 2 mm decrease in Z_{COG} is observed, even though P_{ratio} is still 1%. This result suggests that at atmospheric pressure, the thermal impact of NRP sparks plays a key role in the flame anchoring, while the chemical effect of NRP glow discharges is less effective. This is in agreement with previous studies [22, 23], showing that a combined thermal and chemical action has a stronger effect on the combustion process than a purely chemical one.

At 2 bar, for $P_{\text{ratio}} = 1\%$, the efficiency of plasma actuation on the flame anchoring is very similar for a large range of NRP spark percentages, from 15% to 70% (see figures 6(b) and 7(b)). This result suggests that at 2 bar, the flame is not sensitive to the plasma regime and NRP glow discharges become as effective as NRP sparks. This could be explained by either a stronger chemical impact on combustion at elevated pressure or an increase of the thermal impact associated with NRP glow discharges. Indeed, to maintain a given P_{ratio} while increasing pressure, it is necessary to increase the PRF to promote NRP glow discharges instead of NRP sparks (see section 3.5 and figure 9). Recently, Adams *et al* [24] showed that an increase in PRF could significantly increase the thermal impact of similar discharges in air. Further investigation is necessary to conclude. Note that this change in effectiveness between NRP glow and NRP spark discharges at 2 bar has recently been reported in [12] for enhancement of the lean blow-off limit.

At 3 bar, similar conclusions as at 2 bar can be drawn, except for points H and I (see figures 6(c) and 7(c)), obtained for 15 and 16 kV, for which a larger percentage of NRP spark discharges has a negative effect on the flame anchoring. This non-monotonic trend may be explained by considering the strength of the NRP spark discharges generated at elevated pressure.

During the experimental campaign, for 15 and 16 kV applied voltage, strong disturbances of the base of the flame could be observed. Visually, these disturbances correlated with strong discharges (i.e. intense light emission of the discharge filament). Due to the sudden thermal expansion of the gas heated by the discharges, shock waves are produced by NRP spark discharges [20]. These shock waves lose energy rapidly and become acoustic waves, but in the cases of 15 and 16 kV, they may be strong enough to disturb the anchoring of the flame on the central rod. Indeed, the discharges are generated at the close vicinity of the inner recirculation zone, which is known to be a key area for swirl flame stabilization (see for example [25, 26]). Note that these disturbances of the flame base were not observed regularly but more like exceptional events, i.e. a few times per minute.

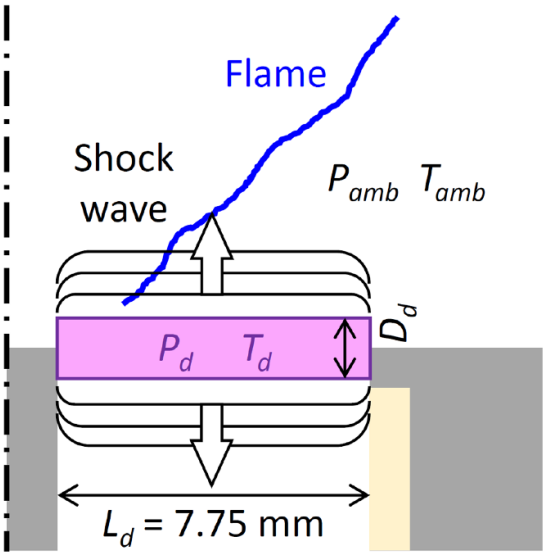

Figure 8. Schematic of the NRP discharge model in the inter-electrode gap. The scale of the discharge is exaggerated to help visualization.

3.4. Hydrodynamic effect of the plasma actuation

In order to verify if at 3 bar for 15 and 16 kV applied voltage, the shock waves produced by NRP sparks could be stronger than for the other conditions, a simple model is proposed here. The strength of the shock wave following an NRP spark, S_{shock}, can be defined as the ratio between the change in pressure across the shock over the ambient pressure, P_{amb} [27]:

$$S_{shock} = \frac{P_d - P_{amb}}{P_{amb}}, \tag{2}$$

where P_d is the pressure in the discharge channel at the end of an NRP spark, that has to be determined. Figure 8 presents a schematic of the situation considered here.

During an NRP spark discharge, the energy is deposited in a very short time and P_d can be calculated considering heating at constant volume of the gas in the discharge channel. For the conditions of this study, the fraction of total energy deposited by the discharges that goes into ultra-fast heating, $E_{thermal}$, is assumed to be 20% of the total deposited energy, as for example in [19]. Only NRP spark discharges are considered in this model. Therefore, $E_{thermal}$ is evaluated from the average energy per pulse deposited by NRP spark discharges at each condition analyzed. The discharge channel is modeled as a cylinder of length L_d equal to the electrode gap distance, *i.e.*, 7.75 mm, and of diameter D_d. The diameter of an NRP spark discharge depends on multiple parameters, including gap distance, gas composition, pressure, and temperature. For a simple model, as the gap distance, gas composition, and temperature do not change much for all conditions, D_d is considered to be only a function of the pressure:

$$D_d = AP_{amb}^{-1} + B, \tag{3}$$

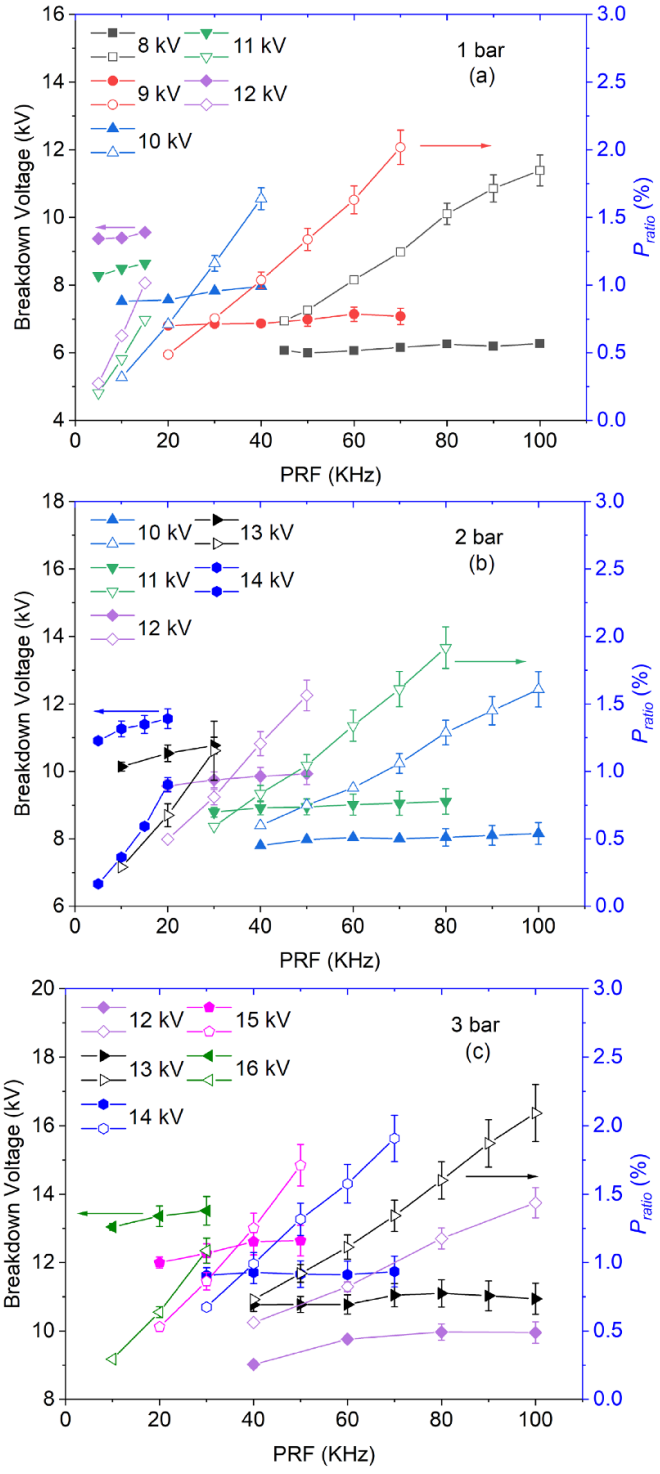

Figure 9. Breakdown voltage (solid symbols) and power ratio (empty symbols) as a function of PRF at 1 (a), 2 (b), and 3 bar (c) for different applied voltages. The error bars represent the standard deviation of the measurements.

where A and B are constants. Assuming discharges in a methane-air mixture at ambient temperature, $T_{amb} = 300$ K, A and B are determined using experimental results from [20, 28]. In [28], Xu *et al* showed that for pressures in the range of 1–5 bar, and for energies per pulse in the range of 1.8–9 mJ,

NRP sparks in lean propane–air mixtures and in air have similar diameters. Here, it is assumed that NRP discharges in lean methane–air mixtures have a diameter similar to that of NRP sparks in lean propane-air mixtures. Furthermore, measurements by a thermocouple in the injection tube, with flame but without plasma actuation, confirmed that, at atmospheric pressure, the average temperature in the inter-electrode area is close to ambient. Depending on the conditions, a maximum average temperature of 350 K was measured. For a pressure in bar and a discharge diameter in millimeter, $A = 0.21$ mm bar and $B = 0.24$ mm. Thus, D_d decreases from 0.45 mm at 1 bar to 0.345 mm at 2 bar, and 0.31 mm at 3 bar. Under these assumptions, and assuming ideal gas conditions, P_d is calculated from:

$$P_d = \frac{T_d}{T_{\text{amb}}} \times P_{\text{amb}} = \frac{\frac{E_{\text{thermal}}}{m\,c_v} + T_{\text{amb}}}{T_{\text{amb}}} \times P_{\text{amb}}, \qquad (4)$$

where c_v is the specific heat at constant volume of the methane–air mixture at T_{amb}, and m is the mass of gas in the discharge volume.

Table 2 summarizes the values of D_d and S_{shock} obtained for six data points of interest. Points E, F, and G feature the same applied voltage (12 kV) and P_{ratio} ($\approx$1%) for ambient pressures of 1, 2, and 3 bar, respectively. While E_{thermal} slightly increases with pressure, the strength of the shock S_{shock} slightly decreases from 1.7 to 1.4, and the effect on the flame anchoring is similar for these three conditions with $Z_{\text{COG}} \approx 22.5$ mm (see figure 6).

Points H and I correspond to the strongest plasma actuation obtained with 15 and 16 kV for a flame at 3 bar (see figure 6). For these two points, the shocks generated by the NRP spark discharges are significantly stronger than for lower applied voltage, with $S_{\text{shock}} = 2.4$ and $S_{\text{shock}} = 2.6$, respectively. The shock waves generated by the NRP sparks for these conditions may be powerful enough to disturb the base of the flame and to have a negative impact on flame anchoring.

The simple model used here does not account for the full complexity of the experiments. However, it suggests that at elevated pressures, the ultra-fast heating associated with NRP spark discharges may have a negative impact on flame actuation. More detailed modeling, including the gas mixture complexity in the inter-electrode area, multi-dimensional effects such as bending of the spark discharge due to the turbulent swirling flow and shock wave-induced flow structures, the effect of the experimental conditions on the fraction of total energy that goes into ultra-fast heating, and a more precise evaluation of the discharge diameters should be performed to confirm this result.

3.5. Plasma actuation strategies

To compare the different plasma actuation strategies using NRP discharges, it is important to determine the most relevant parameters. At the combustion system level, the actuation efficiency is key, but the robustness and the integration of the plasma actuator are also important. To optimize all these aspects, actuation by NRP discharges offers four levers: the pulse duration, the applied voltage, the pulse repetition frequency, and the location of the discharges in the combustion system. In this study, only the applied voltage and the PRF have been varied. Their effects on the plasma actuation strategies are discussed here.

As discussed in section 3.2, applying a plasma power around 1% of the thermal power released by the flame is a good compromise between the deposited power and an efficient plasma actuation by NRP discharges at pressures between 1 and 3 bar. For $P_{\text{ratio}} > 1\%$, any additional increase in plasma power will have a marginal effect on the flame anchoring. Moreover, the percentage of NRP sparks impacts the effectiveness of plasma actuation. For a given PRF, an increase of the applied voltage will increase the percentage of NRP sparks versus NRP glow discharges. Similarly, for a given P_{ratio}, an increase in applied voltage will increase the percentage of NRP sparks (see figure 7). Therefore, there is value in utilizing high applied voltage.

However, higher applied voltages are prone to generate high electro-magnetic interference (EMI). For this issue, the applied voltage is an important factor and it should be minimized. The minimal voltage that must be applied to obtain a plasma actuation is the breakdown voltage. Therefore, it is also important to determine how the applied voltage and the PRF will affect the breakdown voltage.

The breakdown voltage and the power ratio measured as a function of the PRF are reported in figure 9, for all applied voltages at 1 (a), 2 (b), and 3 bar (c). For all experimental conditions, at constant applied voltage, the breakdown voltage is practically constant with increasing PRF. This means that the synergistic effect of multiple pulses that may be reached for high PRF does not have a strong influence on the breakdown voltage, for the experimental conditions of this study. On the other hand, the breakdown voltage increases with the applied voltage. This is induced by the sharp rise time of the voltage pulse, within 2 ns. As this rise time is constant, the temporal gradient of the voltage increases with the applied voltage (for example, from 4 kV/ns at 8 kV to 6 kV/ns at 12 kV). For all applied voltages, the breakdown voltage is always lower than the applied voltage. Therefore, the breakdown occurs during this sharp gradient. This difference in gradient impacts the breakdown process and, as expected, a higher gradient induces a higher breakdown voltage [29]. Finally, at all pressures, at constant applied voltage, P_{ratio} increases with PRF, and at constant PRF, P_{ratio} increases with the applied voltage.

At 1 bar, for $P_{\text{ratio}} = 1\%$, the most efficient plasma actuation is obtained for the highest applied voltage (12 kV) and a low PRF (15 kHz), as shown in figure 6. Unfortunately, this setting gives the highest breakdown voltage (9 kV), i.e. the worst condition for EMI. Consequently, the selection of PRF and applied voltage will be a compromise between the most efficient plasma actuation and the control of EMI.

At 2 bar, for $P_{\text{ratio}} = 1\%$, the efficiency of plasma actuation is not very sensitive to the applied voltage (see figure 6). Therefore, as the lowest breakdown voltage is obtained for low applied voltage, the optimized plasma actuation strategy will be to promote a high PRF and a low applied voltage. In this study, the best plasma actuation strategy is to apply 10 kV

Table 2. Summary of calculated discharge diameter, D_d, and strength of the shock, S_{shock}, for five conditions highlighted in figures 6 and 7.

Point	$V_{applied}$ (kV)	PRF (kHz)	$E_{thermal}$ (mJ)	P_{amb} (bar)	D_d (mm)	S_{shock}
E	12	15	0.54	1	0.450	1.7
F	12	40	0.58	2	0.345	1.6
G	12	80	0.61	3	0.310	1.4
H	15	50	1.06	3	0.310	2.4
I	16	30	1.16	3	0.310	2.6

pulses at 70 kHz. The flame actuation will then be optimal (with a $P_{ratio} = 1\%$ and a flame fully anchored), and the breakdown voltage will be minimal (8 kV). Note that the best plasma actuation strategy at 2 bar will be achieved for an applied voltage lower than the applied voltage necessary to obtain the most effective plasma actuation at 1 bar (12 kV).

Finally, at 3 bar, conclusions are similar as at 2 bar: the best plasma actuation strategy will be to choose pulses of low applied voltage at high repetition frequency. In this study, this corresponds to 12-kV applied voltage and a PRF of about 75 kHz, for which the breakdown voltage will be as low as 10 kV, and the flame will be fully anchored for $P_{ratio} = 1\%$.

These results at pressures up to 3 bar show that high values of applied/breakdown voltage are not always necessary for an efficient plasma actuation strategy, while the repetition frequency of the pulses may be a key factor for flame actuation at elevated pressure.

4. Conclusion

The efficiency of plasma actuation of premixed swirl flames by NRP discharges has been investigated at pressure up to 3 bar. Various combinations of applied voltage and PRF have been investigated. Images of OH^* chemiluminescence from the flames have been collected and analyzed to assess the effect of NRP plasma discharges on the average position of the center of gravity of the flame. The main findings are:

- For pressures between 1 and 3 bar, the most efficient plasma actuation of the flame is obtained for a ratio between the plasma power deposited by NRP discharges and the thermal power released by the flame of about 1%. Above 1%, adding more plasma power has only a marginal effect on flame anchoring.
- At atmospheric pressure, for a given plasma power, the plasma actuation is more efficient for elevated applied voltages, *i.e.* when the percentage of NRP sparks versus NRP glow discharges is high.
- At 2 and 3 bar, the discharge regime, controlled by the applied voltage, had little influence on flame anchoring, suggesting that NRP glow discharges can be as efficient as NRP sparks for flame actuation at elevated pressure. This finding is in agreement with the results presented in [12] where it has been shown that NRP glow discharges are as effective as NRP spark discharges in extending the lean blow-off limit of swirl flames at pressures above 2 bar.
- At 3 bar, for applied voltages of 15 and 16 kV, the plasma effect on flame anchoring is less pronounced than for lower applied voltages. Strong shock waves generated by the NRP sparks obtained for these conditions may be responsible for the flame destabilization, and the limited benefit on flame anchoring.
- While for swirl flames at atmospheric pressure the best strategy for plasma actuation is to increase the applied voltage and control the plasma power by setting a low pulse repetition frequency, at 2 and 3 bar, it is more efficient to choose the lowest applied voltage required for breakdown and to adjust the plasma power by increasing the pulse repetition frequency. This result is promising for plasma actuators targeting high-pressure combustion systems such as gas turbine engines.

Acknowledgments

This work is funded by the King Abdullah University of Science and Technology, the Deutsche Forschungsgemeinschaft, and the Agence Nationale de la Recherche, through the GECCO project.

ORCID iDs

Francesco Di Sabatino https://orcid.org/0000-0003-0038-1395
Deanna A Lacoste https://orcid.org/0000-0002-4160-4762

References

[1] Lieuwen T and Yang V eds 2005 *Combustion Instabilities in Gas Turbine Engines (Progress in Astronautics and Aeronautics* (AIAA, Inc.) vol 210
[2] Mintoussov E, Pancheshnyi S and Starikovskii A 2004 *Proc. 42nd AIAA ASM, Reno, Nevada* AIAA 2004–1013
[3] Choi W, Neumeier Y and Jagoda J 2004 *Proc. 42nd AIAA ASM, Reno, Nevada* AIAA-2004-982
[4] Starikovskaia S M, Kosarev I N, Krasnochub A V, Mintoussov E I and Starikovskii A Y 2005 *Proc. 43rd AIAA ASM, Reno, Nevada* AIAA 2005–1195
[5] Kim W, Mungal M and Cappelli M 2005 *Proc. 43rd AIAA ASM, Reno, Nevada* AIAA 2005–931
[6] Pilla G, Galley D, Lacoste D, Lacas F, Veynante D and Laux C 2006 *IEEE Trans. Plasma Sci.* **34** 2471–7
[7] Dutta A, Yin Z and Adamovich I 2011 *Combust. Flame* **158** 1564–76
[8] Bak M, Do H, Mungal M and Cappelli M 2012 *Combust. Flame* **159** 3128–37
[9] Barbosa S, Pilla G, Lacoste D, Scouflaire P, Ducruix S, Laux C and Veynante D 2015 *Phil. Trans. R. Soc.* A **373** 20140335
[10] Choe J and Sun W 2018 *J. Phys. D: Appl. Phys.* **51** 365201

[11] Kim W and Cohen J 2019 *Combust. Sci. Technol.* 1–20
[12] Di Sabatino F and Lacoste D 2020 *J. Phys. D: Appl. Phys.* **53** 355201
[13] Lacoste D, Moeck J, Durox D, Laux C and Schuller T 2013 *J. Eng. Gas Turbines Power* **135** 101501–1–7
[14] Boyette W, Elbaz A, Guiberti T and Roberts W 2019 *Exp. Therm. Fluid Sci.* **105** 332–41
[15] Di Sabatino F, Guiberti T F, Boyette W R, Roberts W L, Moeck J P and Lacoste D A 2018 *Combust. Flame* **193** 272–82
[16] Pai D, Stancu G, Lacoste D and Laux C 2009 *Plasma Sources Sci. Technol.* **18** 045030
[17] Pai D, Lacoste D and Laux C 2010 *Plasma Sources Sci. Technol.* **19** 065015
[18] Lacoste D *et al* 2017 *Combust. Sci. Technol.* **189** 2012–22
[19] Dumitrache C, Gallant A, Minesi N, Stepanyan S, Stancu G and Laux C 2019 *J. Phys. D: Appl. Phys.* **52** 364001
[20] Xu D, Lacoste D, Rusterholtz D, Elias P Q, Stancu G and Laux C 2011 *Appl. Phys. Lett.* **99** 121502
[21] Rusterholtz D, Lacoste D, Stancu G, Pai D and Laux C 2013 *J. Phys. D: Appl. Phys.* **46** 464010
[22] Tholin F, Lacoste D and Bourdon A 2014 *Combust. Flame* **161** 1235–46
[23] Starikovskiy A 2012 *Proc. 50th AIAA ASM, Nashville, TN* AIAA 2012–0244
[24] Adams S, Miles J, Ombrello T, Brayfield R and Lefkowitz J 2019 *J. Phys. D: Appl. Phys.* **52** 355203
[25] Syred N, Chigier N and Beer J 1971 *Symp. (Int.) Combust.* **1** 617–24
[26] Candel S, Durox D, Schuller T, Bourgouin J F and Moeck J P 2014 *Annu. Rev. Fluid Mech.* **46** 147–73
[27] Jones D, Goyer G and Plooster M 1968 *J. Geophys. Res.* **73** 3121–7
[28] Xu D, Lacoste D and Laux C 2016 *Plasma Chem. Plasma Process.* **36** 309–27
[29] Raizer Y P 1991 *Gas Discharge Physics* (Berlin: Springer) pp 324–63